Journal of Alloys and Compounds 495 (2010) 113–115

Contents lists available at ScienceDirect

Journal of Alloys and Compounds

journal homepage: www.elsevier.com/locate/jallcom

Sol–gel synthesis of forsterite nanopowders with narrow particle size distribution

K.P. Sanosh[a,b], A. Balakrishnan[a,b], L. Francis[c], T.N. Kim[a,*]

[a] Department of Information and Electronic Materials Engineering, College of Engineering, Paichai University, Daejeon, 302-735, Republic of Korea
[b] Division of Metrology for Emerging Technology, Korea Research Institute of Standards and Science, 1 Doryong-Dong, Yuseong-Gu, Daejeon 305-340, Republic of Korea
[c] University of Genova, Department of Chemistry and Industrial Chemistry, via Dodecaneso 31, 16146, Genova, Italy

ARTICLE INFO

Article history:
Received 24 August 2009
Received in revised form 19 January 2010
Accepted 21 January 2010
Available online 1 February 2010

Keywords:
Forsterite
Nanopowders
Particle size
Sol–gel
Calcination
Phase purity

ABSTRACT

Forsterite (FS) nanopowders (~27 nm) were synthesized using a sol–gel route with magnesium nitrate hexahydrate and tetra ethyl ortho-silicate as magnesium and silicon precursors, respectively. Nitric acid was used as a catalyst. After aging, the FS gel was calcined at 800 °C for 30 min. The calcined powders were characterized for phase composition using X-ray diffractrometry and fourier transform-infrared spectroscopy. The particle size and morphology was studied using transmission electron microscopy. The particle size distribution analysis of FS powders showed skewed distribution plot with particle size ranging from 5–90 nm. This study showed that high phase purity and narrowly distributed FS nanoparticles could be obtained using this simple sol–gel technique.

1. Introduction

Nanoparticles offer a host of attractive properties which includes increased strength, high hardness, high diffusion rates, and reduced sintering times in comparison to those associated with coarser particles [1–3].

Forsterite (FS, Mg_2SiO_4) is a member of olivine family of crystals in the magnesia–silica system [4,5]. In recent years, FS has gained popularity due to its wide range of applications. For instance, in electronics it is used as an active medium for microwave and tunable laser applications owing to its high melting point at 1890 °C, low dielectric permittivity, chemical stability, and excellent insulation properties even at high temperatures [4–6]. For SOFC (solid oxide fuel cells) applications, FS is an important material since its linear thermal expansion coefficient perfectly matches the other cell components and it exhibits very high stability in fuel cell environments [7]. Besides FS exhibits good biocompatibilty [8,9] and fracture toughness (K_{IC} = 2.4 MPa $m^{1/2}$) (superior to the lower limit reported for cortical bone [10–12]) thereby making it an excellent biomaterial.

Despite the growing demand; the synthesis of pure nanocrystalline FS with controlled particle size has remained a challenge. This is mainly because the reaction of the starting oxides to form silicate is generally slow due to the relatively low diffusivity which results in the formation enstatite ($MgSiO_3$) and/or MgO instead of FS. Hence very high processing temperature of 1200–1600 °C is required [13] resulting in coarse grained powders. Many alternative powder processing techniques have been reported for the synthesis of pure FS, for example mechano-thermal synthesis [14], mechano-chemical synthesis [15] and sol–gel techniques [12,16,17]. Although the techniques adopted in the above works [14–17] reported FS crystallite size in the range of 10–90 nm (this was calculated using X-ray diffraction (XRD) technique), no analysis was reported on the particle size distribution of the synthesized powder. Considering the calcination temperature (typically 800–1000 °C) and time (2–3 h) applied in these processing methods, we believe that the particles could have been subjected to aggregation (i.e. particle sintering) due to high surface energy. This can broadly distribute the particle size range from nano to submicronic scale. Keeping the above points in view, in the present work FS nanopowder is synthesized using a simple sol–gel based method. Besides the simplicity, the advantage of this technique is that the synthesized FS powder (~27 nm) is narrowly distributed and controlled over a size range of 5–90 nm.

2. Material and methods

Magnesium nitrate hexahydrate ($Mg(NO_3)_2{\cdot}6H_2O$) (MNH) (Junsei chemicals Co., Ltd., S. Korea) and Tetra ethyl ortho-silicate (TEOS) (Acron Organics, USA) were used as starting magnesium and silicon precursors. About 8.5 g of TEOS was dissolved in 300 ml of 1 M HNO_3. To this solution 20.5 g of MNH was added and stirred for

* Corresponding author. Tel.: +82 42 520 5740; fax: +82 42 520 5740.
E-mail address: the_krecian@yahoo.com (T.N. Kim).

0925-8388/$ – see front matter © 2010 Elsevier B.V. All rights reserved.
doi:10.1016/j.jallcom.2010.01.097

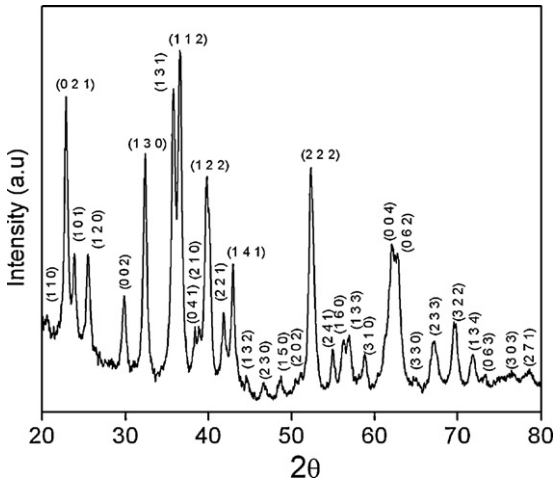

Fig. 1. XRD analysis of FS nanopowders calcined at 800 °C for 30 min.

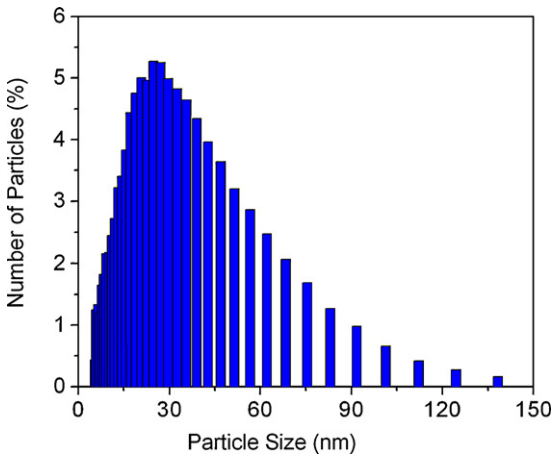

Fig. 2. PSD analysis of calcined FS nanopowders.

2 h at room temperature. The pH of the solution was measured to be about 4. This stirred solution was kept in dry oven and aged at 65 °C for 12 h to form a highly viscous gel. This highly viscous gel was calcined at 800 °C for 30 min in air using an electrical furnace (Daesung electrics, Korea) and employing a heating rate of 10 °C/min. Transmission electron microscope (TEM) (HRTEM, Model Tecnai-Philips F30, FEI Co., Hillsboro) was used to observe the particle morphology and size of dried and calcined FS powders. Phase analysis was performed by X-ray diffractrometry (XRD) (D8 Advance, Brukeraxs, Germany). The mean crystallite size (D) of the particles was calculated from the XRD line broadening measurement from the Scherrer equation given below [18]

$$D = \frac{0.89\lambda}{\beta \cos\theta} \quad (1)$$

where λ is the wavelength (Cu Kα), β is the full width at the half-maximum of the FS (1 1 2) line and θ is the diffraction angle.

The particle size distribution of the powder was determined using a condensation particle counter (GRIMM Aerosol Technik, Gmbh, Germany (Serial No. 5400)). The fourier transform-infrared spectroscopy (FT-IR) was done with Nexus 6700 FT-IR (Thermo-Nicolet, Inc.) equipped with an attenuated total reflectance (ATR) accessory (Smart Miracle, PIKE Tech.).

3. Results and discussion

Fig. 1 illustrates XRD patterns of calcined gel of forsterite powder at 800 °C for 30 min. It should be noted that the sintering time adopted here is much lower that the techniques reported earlier [12,16,17]. The crystallite size (using Eq. (1)) calculated from XRD for five powder batches were found to be 22 ± 7 nm, respectively. The crystallite size obtained from XRD was in close proximity to PSD analysis (Fig. 2) which showed skewed distribution ranging from 5–90 nm with particle size centered at ~27 nm. It was also observed that less than 2% of the total number of particles showed size above 100 nm. This increase in size could be attributed to the strong aggregation phenomena associated with the high surface area and energy properties of nanoparticles [19]. The morphological shape and size of FS powder obtained from TEM is shown in Fig. 3a. Prolate spheroid shaped particles were formed by this process. Agglomeration (sticking of particles) was observed (Fig. 3b). The average particle size of the FS powders measured from TEM was found to be 25–50 nm which was in agreement with the XRD and PSD analysis.

The reaction and nucleation of FS nanopowders can be given as follows:

$$2Mg(NO_3)_2 \cdot 6H_2O + (CH_3CH_2O)_4Si \xrightarrow{HNO_3} Mg_2SiO_4 + 4CH_3CH_2OH + 8H_2O + 4HNO_3 \quad (i)$$

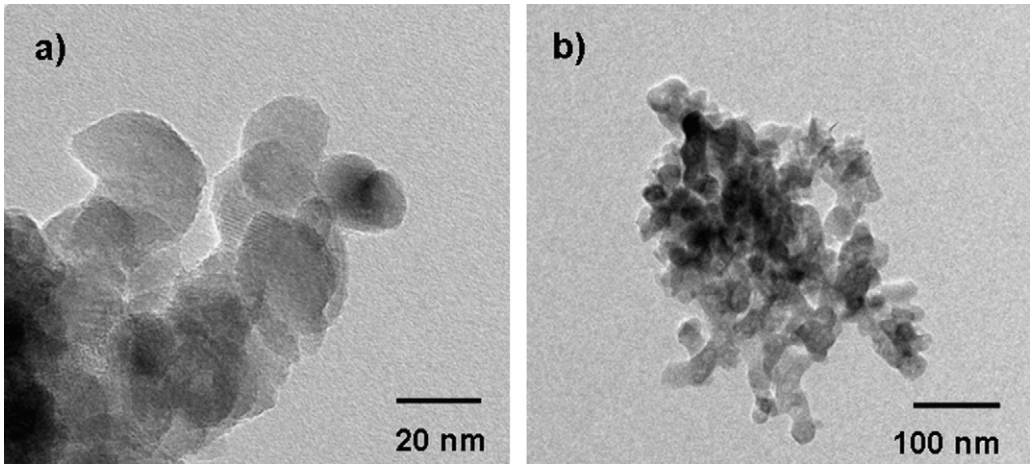

Fig. 3. TEM images of calcined FS nanopowders showing (a) prolate spheroid particles and (b) agglomeration of particles.

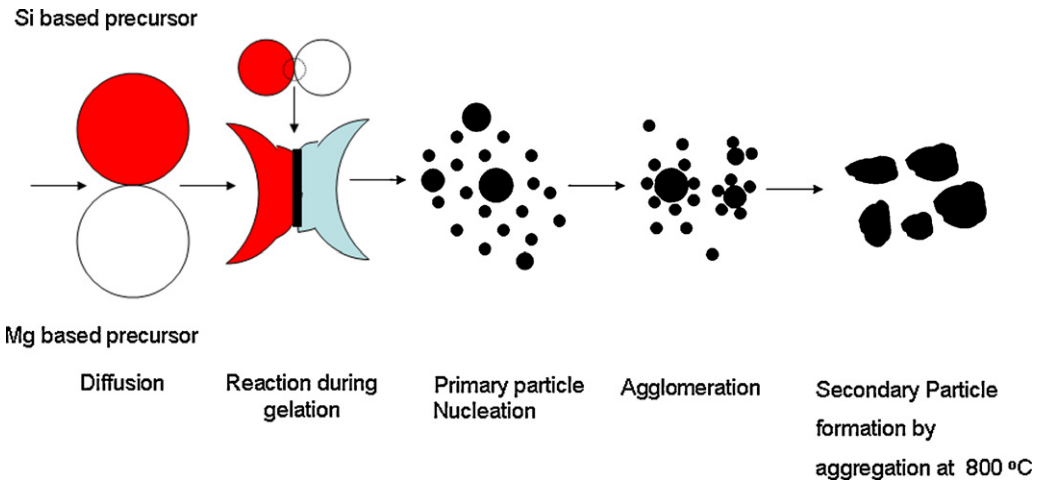

Fig. 4. Nucleation and growth mechanism of FS particles.

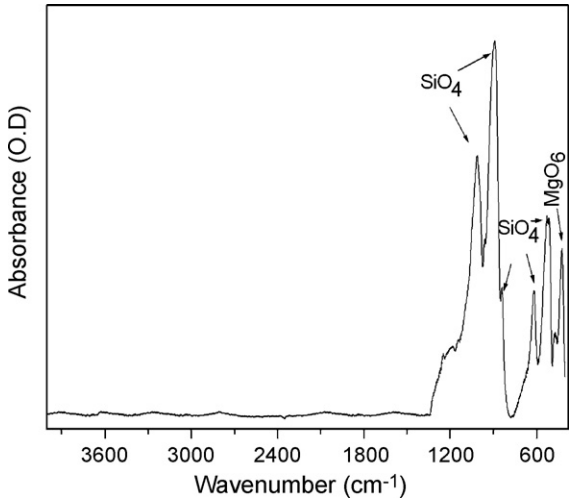

Fig. 5. FT-IR analysis of calcined FS nanopowders.

The nucleation and growth of FS with temperature can be described by nucleation–aggregation–agglomeration-growth mechanism theory explained earlier [20,21]. According to this mechanism, FS particle goes through following steps: (a) nucleation to form amorphous FS nanocrystallites during gelation; (b) agglomeration (sticking) of these crystallites by molecular attractions [22] like van der Waals forces which cause surface free energy minimization (c) van der Waals forces act as cementing agent inside the agglomerates and calcination at 800 °C results in aggregation (fusing of agglomerated particles by bonded necks) to form secondary particle. This mechanism has been schematic represented in Fig. 4.

FT-IR analysis (Fig. 5) shows peaks of Si–O bands in the SiO_4 tetrahedron that prove the formation of FS as it is shown in XRD pattern of this sample (Fig. 1). No secondary bands were observed indicating that the FS powders were of pure nature. The bands related to the characteristic peaks of FS appear in the range of 830–1007 cm^{-1} (SiO_4 stretching), at 500–620 cm^{-1} (SiO_4 bending) and at 420 cm^{-1} for modes of octahedral MgO_6 were observed. The bands were in agreement to earlier reported work [15].

4. Conclusions

In this study, the synthesis of a nanosized FS powder via sol–gel method is reported using Mg and Si based precursors. This process showed that high purity product of nano-FS powders could be obtained by this simple process. Particle distribution analysis showed a skewed distribution plot where the particle size was centered at ~27 nm. TEM analysis showed the nanoparticles to be of prolate spheriodal structure. XRD analysis revealed the powder to be pure and crystalline. FT-IR results showed SiO_4 and MgO_6 bands characteristic for the formation of FS. FS nanopowder synthesized here is expected to have better bioactivity and sinterability than coarser crystals. Future work is focused on the controlled sintering of these nanoparticles to obtain high strength material for structural and biomedical applications.

References

[1] M. Tavoosi, M.H. Enayati, F. Karimzadeh, J. Alloys Compd. 464 (2008) 107–110.
[2] L. Zhenglong, L. Zuyan, C. Yanbin, J. Alloys Compd. 470 (2009) 470–472.
[3] G.L. Tan, J.H. Du, Q.J. Zhang, J. Alloys Compd. 468 (2009) 421–431.
[4] T.S. Sasikala, M.N. Suma, P. Mohanan, C. Pavithran, M.T. Sebastian, J. Alloys Compd. 461 (2008) 555–559.
[5] F. Tavangarian, R. Emadi, J. Alloys Compd. 485 (2009) 648–652.
[6] L. Lin, M. Yin, C. Shi, W. Zhang, J. Alloys Compd. 455 (2008) 327–330.
[7] C. Kosaovic, N. Stubicar, N. Tomasic, V. Bermanec, M. Stubicar, J. Alloys Compd. 389 (2005) 306–309.
[8] S. Ni, L. Chou, J. Chang, Ceram. Int. 33 (2007) 83–88.
[9] S. Ni, L. Chou, J. Chang, J. Mater. Sci.: Mater. Med. 19 (2008) 359–367.
[10] M. Knepper, S. Moricca, B.K. Milthorpe, Biomaterials 18 (1997) 1523–1529.
[11] M.H. Fathi, M. Kharaziha, Mater. Lett. 63 (2009) 1455–1458.
[12] M. Kharaziha, M.H. Fathi, Ceram. Int. 35 (2009) 2449–2454.
[13] A. Douy, J. Sol–Gel Sci. Technol. 24 (2002) 221–228.
[14] M.H. Fathi, M. Kharaziha, Mater. Lett. 62 (2008) 4306–4309.
[15] M.H. Fathi, M. Kharaziha, J. Alloys Compd. 472 (2009) 540–545.
[16] S. Ali, A. Babak, N. Zahra, K. Faramarz, A. Ali, Mater. Res. Bull. 42 (2007) 666–673.
[17] A. Kazakos, S. Komarneni, R. Roy, Mater. Lett. 9 (1990) 405–409.
[18] L.A. Azaroff, Elements of X-ray Crystallography, McGraw-Hill, New York, 1968, 38-42.
[19] C.L. Martin, B. Didier, D. Gérard, J. Am. Ceram. Soc. 89 (2006) 3379–3387.
[20] R. Rodrĭiguez-Clemente, A. Lĭopez-Macipe, J. Gĭomez-Morales, J. Torrent-Burguĭes, V.M. Castaĭno, J. Eur. Ceram. Soc. 181 (1998) 1351–1356.
[21] K.P. Sanosh, M.C. Chu, A. balakrishnan, T.N. Kim, S.J. Cho, Bull. Mater. Sci. 32 (2009) 465–470.
[22] J. Gomez-Morales, J. Torrent-Burgues, R. Rodriguez-Clemente, Cryst. Res. Technol. 36 (2001) 1065–1074.